

Article

The Influence of Seamounts on the Enrichment of Rare Earth Elements in Sediments—A Case Study of the Marcus-Wake Seamounts in the Western Pacific Ocean

Tinglu Xiao ^{1,2}, Dong Xu ^{1,2,*} , Tao Deng ^{1,2}, Junyu Lin ^{1,2}, Liming Ye ^{1,2}, Qian Ge ^{1,2}, Xibin Han ^{1,2} , Yanhui Dong ^{1,2}  and Fengyou Chu ^{1,2}

¹ Key Laboratory of Submarine Geosciences, Ministry of Natural Resources, Hangzhou 310012, China; 18144432016@163.com (T.X.); 18922693125@163.com (T.D.); 18320379372@163.com (J.L.); xinshanren@163.com (L.Y.); gq980447@hotmail.com (Q.G.); hanxibin@sio.org.cn (X.H.); luster15991@163.com (Y.D.); chu@sio.org.cn (F.C.)

² Second Institute of Oceanography, Ministry of Natural Resources, Hangzhou 310012, China

* Correspondence: xudong@sio.org.cn

Abstract: Deep-sea sediments enriched in rare earth elements and yttrium (REY-rich sediments) are widely distributed on the deep-sea floor, and their formation mechanism remains elusive. Although studies have recognized the link between seamounts and REY-rich sediments, in-depth analysis of the specific roles and effects of seamounts in the formation of REY-rich sediments is lacking. In this study, we analyzed surface sediments from the Marcus-Wake Seamounts for grain size, geochemistry, and mineral composition and classified the samples into three types: samples with moderate REY content and dominated by terrestrial detritus; samples with high REY and authigenic mineral content; and samples rich in CaCO₃ but poor in REY. The REY in the sediments of the study area partly originate from Asian dust input and partly from seawater and/or pore water, and are mainly enriched in REY carrier particles including bioapatite fossils and micronodules. The amount of REY carrier particles influences the REY content in the sediments. The current field, primary productivity, weathering process, and depositional environment around seamounts are different from those of abyssal plains, which are conducive to the formation of REY-rich sediments. Strong bottom currents may exist in the southeastern direction of some large seamounts (e.g., Niulang Guyot), leading to the selective accumulation of REY-rich bioapatite fossils and micronodules, resulting in the formation of REY-rich sediments.

Keywords: REY-rich sediments; western Pacific Ocean; seamounts; bottom currents



Citation: Xiao, T.; Xu, D.; Deng, T.; Lin, J.; Ye, L.; Ge, Q.; Han, X.; Dong, Y.; Chu, F. The Influence of Seamounts on the Enrichment of Rare Earth Elements in Sediments—A Case Study of the Marcus-Wake Seamounts in the Western Pacific Ocean. *J. Mar. Sci. Eng.* **2024**, *12*, 117. <https://doi.org/10.3390/jmse12010117>

Academic Editor: Antoni Calafat

Received: 28 November 2023

Revised: 26 December 2023

Accepted: 5 January 2024

Published: 7 January 2024



Copyright: © 2024 by the authors. Licensee MDPI, Basel, Switzerland. This article is an open access article distributed under the terms and conditions of the Creative Commons Attribution (CC BY) license (<https://creativecommons.org/licenses/by/4.0/>).

1. Introduction

Rare earth elements (REEs) and yttrium (Y) (termed REY) are essential to high-tech industries. In 2011, Japanese scientists reported REY-rich mud in the Pacific Ocean and suggested that this easily leachable REY-rich mud may represent a promising REY resource for the future [1]. Since then, deep-sea REY-rich sediments have attracted much attention from the international academic and mining communities as potential strategic metal resources. Obvious differences in REY content in sediments exist in different regions of the Pacific Ocean, and the REY-rich sediments with the highest known REY content (nearly 8000 ppm) were found around Minamitorishima (Marcus) Island in the western North Pacific Ocean [1–4].

So far, the formation mechanism of REY-rich sediments is not all clear. Previous studies have suggested that REY enrichment in deep-sea sediments may be related to low sedimentation rates [5–8], high abundance of bioapatite fossils (mainly fish debris) and/or Fe-Mn micronodules in the sediments, oxidized bottom water, strong bottom currents [3,6,7,9,10], or a suitable distance from hydrothermally active areas [8,11]. According to previous

studies on the geochemistry and mineralogy of manganese deposits (nodules and crusts), pore water, bottom water and sediments in the Pacific Ocean, REY could be redistributed in the sediment-bottom pore-water system through the adsorption–desorption processes of Fe-Mn particles, degradation of organic matter, adsorption of bioapatite fossils and reactivation of alumina-silicate components [12–17]. Among these processes, adsorption by bioapatite fossils and micronodules are probably the most important [6,8–10,14,18]. Obviously, the concentration of REY carriers (bioapatite fossils, micronodules, clay minerals, etc.) in sediments determines the REY enrichment in the sediments. However, there is still limited research on the geological processes that control the content of these carriers.

A few recent studies have mentioned that seafloor topography may affect REY enrichment in sediments [9,10,19–21]. Wang et al. found that the surface sediments with high REY content are mainly concentrated around seamounts, and the REY content decreases with increasing distance from the seamounts [20]. Otha et al. also correlates differences in REY content with local variations in topography, which they attributed to the upwelling around the seamounts which led to increased productivity and enrichment of bioapatite fossils, resulting in the formation of REY-rich layers [10]. Compared to abyssal plains, sea and pore water around seamounts have higher REY content [19,21]. However, these studies did not further investigate the relationship between topography and REY enrichment. Results based on numerical simulations and in situ observations indicate that the presence of seamounts affects the bottom current field, and the bottom current velocity is related to the size of the seamounts [22–26]. In addition to creating complex flow fields that affect the sorting of REY carriers in sediments, seamounts also provide large amounts of detrital material to neighboring basins, which are important mediators of REY cycling [19,21].

The Marcus-Wake Seamounts in the western Pacific Ocean have attracted much attention because of the abundance of polymetallic nodules (crusts), and more recently because of the discovery of highly REY-rich mud ($\Sigma\text{REY} > 2000$ ppm) and extremely REY-rich mud ($\Sigma\text{REY} > 5000$ ppm) in this region [6,16,17,27]. However, the formation mechanism and spatial distribution pattern of REY-rich sediments in this region still need to be studied in more detail, especially the role of seamounts in the formation of REY-rich sediments deserves further investigation. Against this background, this paper presents a comprehensive analysis of grain size, elemental geochemistry and mineralogy of surface sediments from the Marcus-Wake Seamounts and attempts to explore the sources and carriers of REY in the sediments as well as the correlation between the seamounts and the enrichment of REY in the sediments.

2. Materials and Methods

2.1. Study Area

The study area is located in the southeastern part of the Marcus-Wake Seamounts, which consist of submarine mountain ranges formed by intraplate volcanism and intraplate tectonics, and of intermountain basins surrounding the seamounts [28,29]. The water depth in the study area is generally more than 4500 m, with the water depth at the summit of the seamounts ranging from 1200 to 2000 m, and the water depth in the intermontane basins ranging from 5000 to 6500 m.

The Marcus-Wake Seamounts are influenced by a variety of ocean currents, including the North Equatorial Current (NEC; [30]), the North Pacific Intermediate Water (NPIW; [31]), and the Lower Circumpolar Deep Water (LCDW; [31–34]), of which the oxygen- and nutrient-rich LCDW is the primary water mass influencing the modern deep-sea environment in this region (see Figure 1). The bedrock of the seamounts in the study area is dominated by basalt and volcanoclastic rocks, and the upper part is covered by Tertiary Holocene sediments, mainly pelagic clay, calcareous ooze, siliceous mud, and volcanic deposits [35–39]. The study area is an enriched area for polymetallic nodules (crusts), and the polymetallic nodules are mainly distributed between water depths of 4500 m and 6200 m and are dominated by medium sized nodules [40,41]. The sedimentation rate in the study area is relatively low [20,27,42].

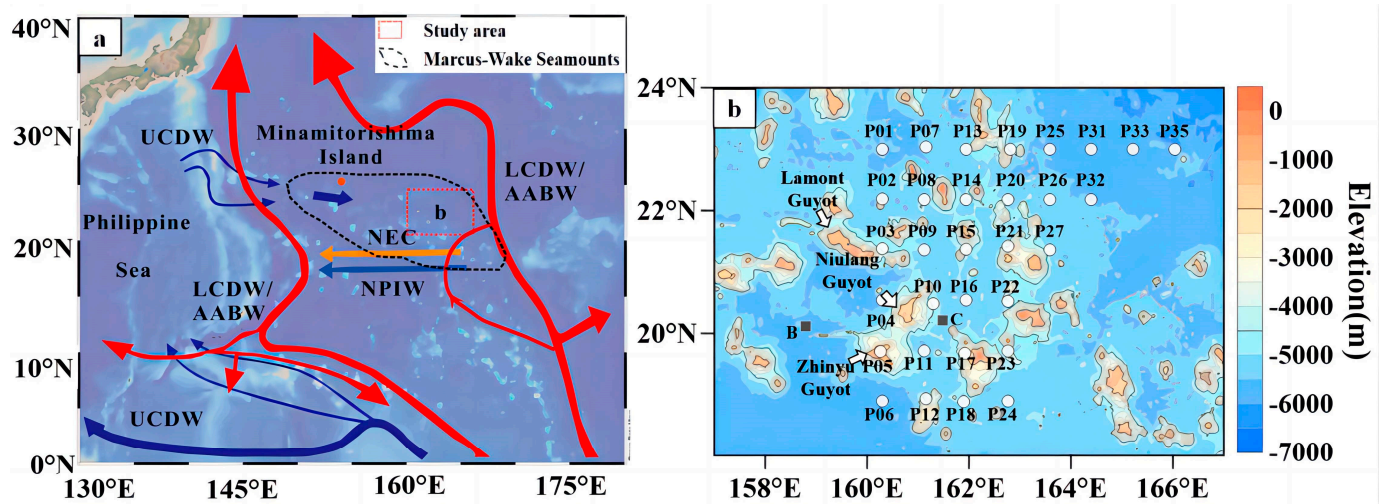


Figure 1. The location of the study area (a) and the distribution of the sampling stations (b). Major ocean currents were modified after [31–35]. NEC: North Equatorial Current; NPIW: North Pacific Intermediate Water; UCDW: Upper Circumpolar dDeep Water; LCDW: Lower Circumpolar Deep Water; AABW: Antarctic Bottom Water. The location of the Marcus-Wake Seamounts after [41], the locations of core B and core C after [6].

2.2. Sample Information

The 31 samples of sediment analyzed in this study were collected with a box sampler by the Second Institute of Oceanography, Ministry of Natural Resources, People’s Republic of China (PRC), during the DY54 cruise in 2019. Sediments in the 0–5 cm depth range of the sampler were used as surface sediments. The information from the sampling stations is shown in Table 1.

2.3. Analytical Method

2.3.1. Grain Size Analysis

Two grain size pretreatment methods, with and without bio-silica removal, were used in this study. The pretreatment steps without removal of bio-silica include: (1) removing organic matter with 30% hydrogen peroxide, (2) removing carbonate with 10% hydrochloric acid, (3) washing three times with deionized water, and (4) dispersing the sample with 10 mL of sodium hexametaphosphate at a concentration of 0.05 mol/L. The major change in the bio-silica removal pretreatment steps is that 10 mL of sodium carbonate at a concentration of 2 mol/L is added between steps 2 and 3 above to remove bio-silica. The grain size analysis instrument used was the Mastersizer 2000 (Malvern, UK), which has a measuring range of 0.02–2000 μm and an analytical accuracy of better than 1%.

2.3.2. Microscopic Identification

Sediment samples were soaked, stirred and sonicated in deionized water, then the fine-grained components were washed out with deionized water on 0.063 mm and 0.25 mm mesh sieves, and the coarse-grained samples on the sieve were collected. We used a stereomicroscope to observe the dried coarse-grained fractions (>63 μm) and qualitatively analyze the mineral composition.

Table 1. Results of grain size analysis, coarse fraction identification and geochemical analysis of surface sediments.

Station	Depth /m	Bb Sand /%	Bb Mz / μ m	Bf Sand /%	Bf Mz / μ m	Tra	Rof	Phi	Fish Teeth	Min	Sbd	For	SiO ₂ /%	Al ₂ O ₃ /%	Fe ₂ O ₃ /%	MnO /%	P ₂ O ₅ /%	CaCO ₃ /%	TOC /%	Co /ppm	Ni /ppm	EREY /ppm
P01	5489	26.18	12.79	0.65	4.41	+	-	-	-	-	+++	-	54.18	14.84	6.85	0.48	0.14	0.43	0.26	56.69	96.04	260.8
P02	4950	3.28	4.34	1.17	4.22	++	+++	++	++	++	++	-	53.13	16.70	8.20	0.64	0.88	0.64	0.27	68.14	153.52	399.2
P03	4763	50.18	38.10	0.03	4.26	-	-	-	-	-	+++	-	55.13	11.98	5.49	0.36	0.23	0.34	0.26	42.94	87.84	271.5
P04	5375	40.75	22.68	0.00	3.95	-	-	-	-	-	+++	-	53.65	15.48	7.28	0.64	0.23	0.51	0.28	77.47	144.32	339.7
P05	1344	12.78	7.56	/	/	-	-	-	-	-	-	+++	1.30	0.73	0.29	0.05	0.06	90.56	0.01	7.54	12.92	58.2
P06	5662	1.39	4.31	0.01	4.07	+	+	+++	+++	+	++	-	51.14	16.26	7.87	0.91	0.49	0.48	0.29	103.04	190.10	558.0
P07	5405	7.47	5.53	0.00	4.36	-	-	-	-	-	+++	-	55.20	14.72	6.80	0.53	0.16	0.36	0.26	57.04	103.76	274.6
P08	5190	5.31	4.88	0.08	4.15	+++	+++	+++	++	++	+	-	53.14	16.34	8.08	0.88	0.74	0.48	0.21	92.90	315.33	586.6
P09	5169	1.16	4.32	0.01	4.33	+	++	+++	++	++	++	-	54.63	16.66	7.63	0.67	0.30	0.35	0.21	73.00	146.98	403.7
P10	4573	0.02	3.90	0.00	4.22	+	++	+++	++	++	++	-	55.32	17.16	7.84	0.57	0.32	0.27	0.22	66.00	144.81	459.8
P11	5364	23.38	10.89	2.99	4.62	+	+++	+++	+++	+++	+	-	50.96	15.84	8.22	1.08	0.99	0.14	0.19	127.47	254.56	913.9
P12	4872	17.95	8.61	4.69	4.29	+	+++	+++	++	+++	+	-	50.73	15.84	7.99	1.12	0.80	0.57	0.24	128.50	281.88	729.3
P13	5451	0.60	3.95	0.00	3.96	-	-	++	++	++	++	-	53.02	16.61	7.63	0.65	0.23	0.82	0.24	72.50	144.94	348.7
P14	5036	0.00	3.74	0.00	3.94	-	-	+	-	++	++	-	53.62	16.73	7.64	0.55	0.22	0.70	0.23	66.44	129.86	346.3
P15	4423	0.40	3.70	0.03	4.24	-	+	+++	+	+	+	+	46.77	14.74	6.62	0.44	0.23	11.58	0.29	53.31	119.58	341.7
P16	5101	1.44	4.61	0.00	4.72	-	+	+	+	+	+++	-	53.21	16.00	7.28	0.60	0.30	0.31	0.26	69.79	143.04	373.5
P17	3303	17.76	8.88	/	/	-	+	++	+	-	+	+++	5.65	1.90	0.84	0.08	0.25	84.50	0.05	9.66	21.16	135.3
P18	5440	0.27	4.12	0.00	4.01	-	+	+++	++	+++	+++	-	51.94	16.57	7.88	0.76	0.37	0.72	0.22	89.30	157.30	432.9
P19	4984	11.73	7.54	0.05	4.23	-	-	+	-	-	+++	-	54.37	16.01	7.25	0.49	0.19	0.49	0.21	56.70	110.67	284.0
P20	5365	0.10	3.73	0.01	4.30	-	-	+	++	+	+++	-	53.11	16.47	7.55	0.60	0.22	0.76	0.24	68.22	141.18	303.6
P21	4623	0.48	3.76	0.00	4.09	+	-	++	++	++	++	-	53.60	16.73	7.68	0.53	0.33	0.77	0.24	66.27	143.36	419.8
P22	4891	0.99	3.96	0.00	3.90	+	-	++	+++	++	+	-	53.63	16.59	7.58	0.59	0.22	0.55	0.27	71.51	148.44	316.9
P23	5029	0.94	4.24	0.00	4.13	-	++	+++	+++	++	+	-	54.10	16.77	7.81	0.58	0.34	0.44	0.25	71.65	142.34	404.7
P24	5258	2.17	4.31	0.00	3.72	-	-	++	+	++	+++	-	51.92	16.30	7.84	0.79	0.37	0.56	0.23	102.31	171.98	443.6
P25	5536	0.02	3.60	0.00	4.17	-	-	+	++	+	+++	-	53.56	16.69	7.65	0.60	0.17	0.76	0.24	77.50	147.81	279.0
P26	5409	0.72	4.88	0.01	4.60	-	-	++	+++	+	+++	-	53.99	16.17	7.23	0.60	0.52	0.91	0.22	75.01	153.75	589.4
P27	4945	0.00	4.11	0.00	3.94	-	-	+	+	+++	+++	-	53.63	16.94	7.68	0.53	0.19	0.45	0.21	61.39	126.18	290.4
P31	5762	0.00	3.69	0.00	3.77	+	-	-	-	+	+	-	53.03	16.85	7.62	0.48	0.15	0.41	0.23	69.89	120.24	258.3
P32	5536	0.11	4.48	0.00	4.26	+	-	++	++	+++	+++	-	53.13	16.29	7.37	0.55	0.35	0.65	0.26	73.91	146.37	419.8
P33	5719	0.00	3.47	0.00	3.95	++	-	+	++	++	+++	-	53.51	16.92	7.66	0.53	0.17	0.70	0.23	73.14	130.19	260.5
P35	5114	0.00	3.47	0.00	3.86	++	+++	++	++	++	++	-	54.01	17.22	7.61	0.48	0.21	0.52	0.20	62.46	127.71	295.9

Abbreviations: Bb = biosilicone bearing; Bf = biosilicone free; Tra = transparent mineral; Rof = rock fragment; Phi = phillipsite; Min = micronodule; Sbd = siliceous biogenic detritus; For = foraminifer. “-” means not found, “+” means little, “++” means moderate, “+++” means abundant, “/” means no data.

2.3.3. Element Analysis

The major elements content of each sample were determined by X-ray fluorescence (XRF) spectrometry. The sample pretreatment process was as follows: (1) the 200-mesh powdered bulk sample was dried at 110 °C for 6 h; (2) about 0.5 g of the above dried sample was weighed into a constant weight ceramic crucible, burned in a muffle furnace at 1000 °C for 180 min, and then weighed and calculated the loss on ignition after cooling to room temperature; (3) the well mixed 0.6000g of the above dried sample and 6.0000 g flux (49.75% $\text{Li}_2\text{B}_4\text{O}_7$: 49.75% LiBO_2 : 0.5% LiBr) were poured into a platinum crucible dedicated to XRF, and then placed in the melting furnace at 1100 °C; (4) after the melting program was completed, the crucible was shaken to expel air bubbles and allow the melt to fill the bottom of the crucible, then the cooled piece of glass was removed, labeled, and prepared for testing. The standard material (AGV-2, W-2a, BHVO-2, BCR-2) for quality control was also prepared using the above procedure, and the analytical precision was better than 5%. A Parnaco Zetium XRF was used for the XRF analysis.

The total carbon (TC) and total nitrogen (TN) content of the whole sample and the total organic carbon (TOC) content of the sample after carbonate removal were measured using a Thermo Fisher elemental analyzer (Flash 2000 CHNS/O, Thermo Fisher Scientific, Waltham, MA, USA). The carbonate content was calculated using the following formula: $\text{CaCO}_3 = (\text{TC} - \text{TOC}) \times 8.33$.

Trace elements were analyzed by inductively coupled plasma mass spectrometry (X Series2 ICP-MS, Thermo Fisher Scientific, Waltham, MA, USA). Approximately, 50 mg of sample was first placed in a pre-purified Teflon beaker, to which distilled and concentrated HNO_3 -HF mixture (1:4) was added. The solution was then dried to evaporate the HF and the residue was redissolved in concentrated HNO_3 and 1:1 HNO_3 and dried again. The sample was then dissolved in 3 mL of 2N HNO_3 solution and then diluted with 2% HNO_3 to a fixed volume for analysis. Standard W-2a and BHVO-2 were used as the reference standard and the analytical precision of most trace elements was better than 10%. Instrument drift was corrected with internal standards and external reference samples. The REY content was calculated using the following formula: $\Sigma\text{REY} = \text{REEs} + \text{Y}$.

The major and trace elements were analyzed at the Key Laboratory of Submarine Geosciences of the Ministry of Natural Resources, while the organic carbon and nitrogen were analyzed at Guizhou Tongwei Analytical Technology Co., Ltd. in Guiyang, China.

3. Results

3.1. Grain Size

Grain size analysis of samples without biogenic silica removal shows that most of the surface sediments are clayey silt ($n = 20$), followed by silty clay ($n = 8$). Silty sand ($n = 2$) and sand-silty-clay ($n = 1$) are present to a lesser extent. The sand content ranged from 0.00% to 50.18% with a mean of 7.34%, the silt content from 38.45% to 58.15% with a mean of 49.09%, and the clay from 10.97% to 54.11% with a mean of 43.57%. The mean grain size (Mz) ranged from 3.74 μm to 38.10 μm with a mean of 6.84 μm .

Notably, grain size analysis of samples with bio-silica removal shows that most of them are silty clay ($n = 27$), followed by clayey silt ($n = 2$). The sand content ranged from 0.00% to 4.69% with a mean of 0.34%, the silt content ranged from 41.00% to 51.62% with a mean of 45.59%, and the clay content ranged from 46.19% to 56.41% with a mean of 51.61%. The mean grain size (Mz) ranged from 3.72 μm to 4.72 μm with a mean of 4.16 μm .

Compared to the samples without biogenic silica removal, the sand content of the samples with biogenic silica removal decreased significantly, the silt content increased, but the Mz decreased, indicating that many samples had high contents of siliceous biogenic detritus with larger grain size; alternatively, the biogenic silica was acting as cement, binding (aggregating) finer particles together. Detailed grain size data is presented in Supplementary Table S1.

3.2. Mineralogical Characteristics of Coarse Fractions

The coarse fraction (>63 μm) of the surface sediments consist mainly of micronodules, fish teeth, phillipsites, siliceous biogenic detritus, etc., with rock fragments, colored transparent minerals, and foraminifers also occurring in some samples (Table 1 and Figure 2).

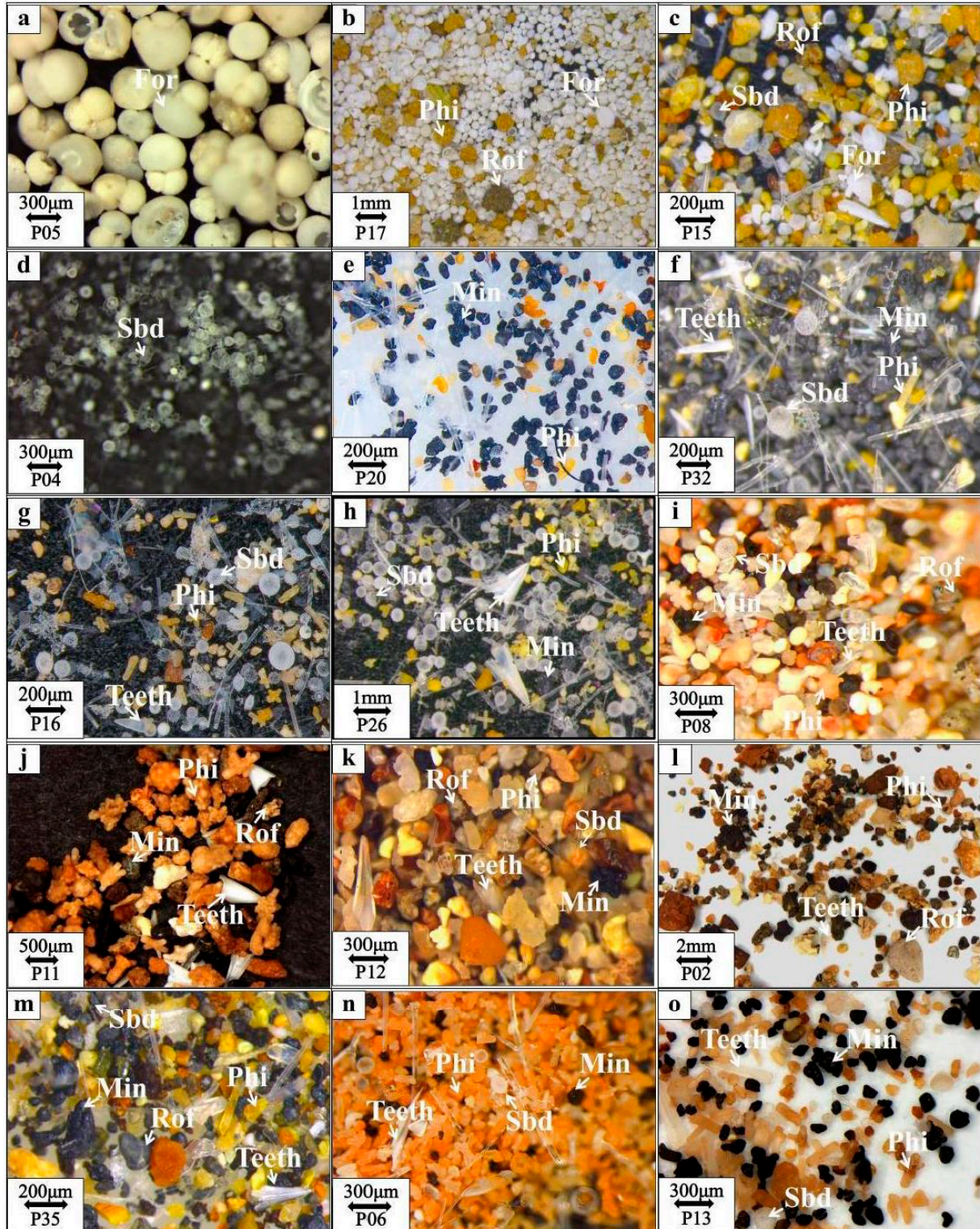


Figure 2. Representative microscopic photos of coarse components of surface sediment samples. (a–c) abundant calcareous shells; (d) rich in siliceous biogenic debris; (e,f), abundant siliceous biogenic

detritus and micronodules; (g,h) dominated by siliceous biogenic detritus and phillipsites; (i–m) diversified coarse grains include rock fragments, phillipsites, fish teeth, micronodules, and minor siliceous biogenic detritus; (n) dominated by phillipsites; (o) dominated by micronodules and phillipsites. Abbreviations: Phi = phillipsite; Min = micronodule; Rof = rock fragment; For = foraminifer; Sbd = siliceous biogenic detritus.

Shallow water (water depth < 4500 m) stations (P05, P15, and P17) contain intact calcareous shells, while calcareous shells decrease with increasing water depth (Figure 2a–c). Samples containing almost exclusively siliceous biogenic detritus in the coarse fraction (P01, P03, P04, P07) are mainly located in the northwestern part of the study area (Figure 2d), while samples with abundant siliceous biogenic detritus and micronodules (P14, P20, P24, P25, P27, P31, P32, P33) are mainly located in the northeastern abyssal plain (Figure 2e,f). There are also samples dominated by siliceous biogenic detritus and phillipsites (P16, P19, P26) (Figure 2g,h).

P11 and P12 have the highest mineral content and diversity, both rich in rock (mainly volcanic clastic rock) fragments, phillipsites, fish teeth, and micronodules, as well as small amounts of siliceous biogenic detritus (Figure 2i–k). The same composition can be seen in P08, P02, and P35 (Figure 2i,l,m).

3.3. Elemental Composition of Sediments

The surface sediments had a wide range of major and trace element contents. The SiO₂ content varies from 1.32% to 55.32% with a mean of 49.30%, and the high content occurs in samples with high content of siliceous biogenic detritus. Al₂O₃ content reflects the contribution of clay minerals and varies from 0.73% to 17.22% with a mean of 15.31%. CaCO₃ content varies from 0.14% to 90.56% with a mean of 6.51%. High CaCO₃ contents occurred at shallow water stations with water depths less than the carbonate compensation depth (CCD), including P05, P15, and P17. Except for two shallow-water samples (P05 and P17), most of the metallic elements (e.g., Mo, Co, Ni, Cu, Zn, etc.) are several or even tens of times higher than upper crustal values [43]. The detailed geochemical results are listed in Supplementary Table S2.

The Σ REY varies from 58.18 ppm to 913.85 ppm, with an average of 380.61 ppm. The Post-Archean Australian Shale (PAAS) [44] normalized indices such as (La/Yb)_{PAAS}, (La/Sm)_{PAAS}, and (Gd/Yb)_{PAAS} with mean values of 0.69, 0.70, and 1.19, respectively, indicate that the sediments are characterized by a relative enrichment of heavy rare earth elements (HREEs). PAAS-normalized δ Ce varies from 0.34 to 1.47 with a mean of 0.98, and δ Eu varies from 1.04 to 1.09 with a mean of 1.06.

The TOC content varies from 0.01% to 0.29% with a mean of 0.23%, while the TN content varies from 0.02% to 0.10% with a mean of 0.06%, which was related to the low primary productivity and poor organic matter preservation conditions in the study area.

4. Discussion

4.1. Factors Controlling the Chemical Composition of Sediments

Previous studies have shown that the sediments in the Marcus-Wake Seamounts have multiple sources, including Asian dust, marine authigenic minerals, seamount weathering material, and biogenic debris [35–39]. In the present study, micronodules, phillipsites, fish teeth, siliceous and calcareous biogenic detritus, volcanic glass, and rock fragments from nearby seamounts were observed in the coarse fraction of the surface sediments, suggesting a polygenic origin of the sediments, which is consistent with previous results.

To further understand the controlling factors of the chemical composition of the Marcus-Wake Seamounts sediments, R-type factor analysis based on normalized geochemical data and correlation analysis were conducted using SPSS18 software. The Kaiser–Meyer–Olkin (KMO) test value of the factor analysis was 0.81, and the variances of the extracted common factors were all greater than 0.7, indicating that the results of the factor analysis had good credibility. After extracting the eigenvalues greater than 1 and rotating them by

orthogonal rotation with large variance, three principal factors were obtained, and the total variance contribution was 89.28%.

The variance contribution of the F1 factor is 50.654% (Table 2), indicating that it plays a decisive role in the geochemical composition of the samples. The positive loadings of F1 factor include SiO₂, TiO₂, Al₂O₃, Fe₂O₃, MgO, Na₂O, K₂O, Th, TOC, and TN, most of them are closely related to detrital minerals and clay minerals sourced from continent and/or marine volcano [45]. The negative loadings of F1 factor include CaO, CaCO₃, and Sr, which are mainly from biological deposition in deep marine sediments. Therefore, the F1 factor can be considered to mainly represent the contribution of terrestrial and seamount-derived detritus and local calcareous biogenic detritus to the geochemical composition of the sediments.

Table 2. R-type factor analysis results of major and trace elements in surface sediments.

Element	Principal Factor			Common Factor Variance
	F1	F2	F3	
SiO ₂	0.957	0.260	0.026	0.985
TiO ₂	0.814	0.553	0.080	0.974
Al ₂ O ₃	0.895	0.370	0.177	0.969
Fe ₂ O ₃	0.851	0.487	0.130	0.979
MnO	0.390	0.891	−0.077	0.952
MgO	0.946	0.306	0.063	0.993
CaO	−0.949	−0.303	−0.026	0.993
Na ₂ O	0.637	0.013	−0.523	0.680
K ₂ O	0.897	0.369	0.149	0.962
P ₂ O ₅	−0.066	0.874	−0.140	0.788
CaCO ₃	−0.942	−0.324	−0.021	0.993
TOC	0.901	0.142	−0.004	0.832
TN	0.871	0.075	0.019	0.765
Co	0.426	0.863	−0.056	0.929
Ni	0.303	0.902	−0.040	0.908
Cu	0.480	0.837	0.018	0.932
Sr	−0.949	−0.282	−0.001	0.980
Mo	0.481	0.709	0.009	0.734
Cd	0.267	0.846	0.207	0.830
Ba	0.244	−0.109	0.780	0.680
Th	0.790	0.478	0.188	0.888
ΣREY	0.164	0.929	−0.055	0.894
variance contribution	50.654%	33.729%	4.897%	89.280%

The variance contribution of the F2 factor is 33.729%, and its combinations are MnO, P₂O₅, Co, Ni, Cu, Mo, Cd, and ΣREY. Mn, Co, Ni, and Cu are the main mineralizing or associated elements of marine authigenic minerals, such as Fe-Mn micronodules, which are closely related to seawater sources [36]. The P in marine sediments can originate from riverine inputs, atmospheric deposition, volcanic activity, and biological effects [46]. Deep-sea REY-rich sediments generally have high levels of bioapatite fossils and micronodules [6,8–10,14,18,35–39]. Therefore, the F2 factor may represent a combination of seawater-derived elements influenced by authigenic minerals (e.g., micronodules) and bioapatite fossils enrichment.

The F3 factor has a variance contribution of 4.897% and the only corresponding element is Ba. The major sources of Ba in marine sediments include terrestrial detrital inputs, biogenic and hydrothermal precipitation, and a small amount of Ba is incorporated or adsorbed in carbonates, opal or Fe-Mn oxides [47,48]. In hydrothermal mid-ocean ridges and back-arc basins, Ba interacts with seawater sulfate to form barite. Biogenic Ba is mostly in the form of microcrystalline barite, which can account for more than 50% of the total Ba content of non-clastic particles in deep-sea sediments [48]. The Ba in the surface sediments of the study area is not significantly correlated with the terrestrial component, biogenic

component, and authigenic Fe-Mn minerals, suggesting that the source and distribution of Ba are complex.

4.2. Sources and Carriers of REY

REE fractionation parameters are often used as source indicators because REEs are not easily fractionated during weathering, transport, and deposition and retain information about the source area [49,50]. The absolute values of the correlation coefficients between the REE fractionation parameters ($(\text{Gd}/\text{Yb})_{\text{PAAS}}$, $(\text{La}/\text{Sm})_{\text{PAAS}}$, and $(\text{Sm}/\text{Nd})_{\text{PAAS}}$) and the chemical index of alteration (CIA) are less than 0.06, the absolute values of the correlation coefficients between the REE fractionation parameters ($(\text{Gd}/\text{Yb})_{\text{PAAS}}$, $(\text{La}/\text{Sm})_{\text{PAAS}}$, and $(\text{Sm}/\text{Nd})_{\text{PAAS}}$) and Mz are less than 0.25 (see Table S3), indicating that the REE fractionation is less affected by weathering [51], and grain size [52]. After standardization of the geochemical data and based on the Q-clustering method, the 31 samples were classified into three classes: Class I are the sediments with moderate REY content dominated by the contribution of terrestrial derived materials ($250 \text{ ppm} < \Sigma\text{REY} < 460 \text{ ppm}$, $n = 24$); Class II are sediments rich in REY and authigenic minerals ($\Sigma\text{REY} > 550 \text{ ppm}$, $n = 5$); and Class III are CaCO_3 -rich and REY-poor sediments ($\Sigma\text{REY} < 250 \text{ ppm}$, $n = 2$) (Table S4). The PAAS-normalized REY partition curves and partition parameters of these three types were compared with those of Asian dust, Marcus-Wake Seamounts bottom water, volcanic debris, and typical REY-rich carriers [6], and the results are shown in Figures 3 and 4.

Most of the samples in this study belong to class I. The REY partitioning curves of these samples are relatively flat, with very weak positive Y anomalies and insignificant Ce and Eu anomalies, and their REY partitioning patterns are similar to those of Asian dust [53–58] and non-REY-rich sediments ($250 \text{ ppm} < \Sigma\text{REY} < 400 \text{ ppm}$) near Minamitorishima Island [6,16,17]. In addition, the Class I REY curves are somewhat similar to those of the micronodules, which usually present obvious positive Ce anomalies [6,59,60], but the ΣREY and Ce anomaly values of Class I are significantly lower than that of micronodules (Figure 3). So, we suppose that the REY in this class mainly originated from the input of Asian dust, with a small contribution from micronodules, bioapatite fossils and other components (as indicated by the existence of micronodules, bioapatite fossils in coarse component, Table 1 and Figure 2).

The Class II sediments have a high REY content, with obvious negative Ce anomalies and positive Y anomalies (Figure 3), and are relatively enriched in medium-heavy REEs, with REY partitioning curves very similar to those of the REY-rich sediments off Minamitorishima Island ($\Sigma\text{REY} > 500 \text{ ppm}$) [6,16,17]. Previous studies have confirmed that the REY partitioning characteristics of REY-rich sediments are largely contributed by bioapatite fossils in the sediments [6]. Compared to Class I sediments, Class II sediments are less affected by the dilution effect of Asian dust (Figure 4), and the coarse fraction has a higher content of REY-rich carriers such as bioapatite fossils and micronodules [6]. Therefore, the REY in this class is mainly contributed by bioapatite fossils, whose REY are intrinsically derived from seawater and/or pore water [6,22,37].

Class III sediments have low REY content, and their REY partitioning curves are similar to those of bottom seawater [36]. This is because these sediments are dominated by calcareous shells, which may have inherited the REY signals from seawater and diluted the REY signals from dust, bioapatite fossils, and micronodules.

Previous studies have generally concluded that bioapatite fossils, represented by fish teeth, are the primary and ultimate host for REY, and that Fe-Mn oxides/hydroxide, represented by micronodules, are temporary “sinks” for REY [19,59–63]. During the early stages of sedimentation, sediments mainly rely on Fe-Mn oxides for REY uptake, but during early diagenesis, REY migrate between bioapatite fossils and Fe-Mn oxides [8,59–63], and REY (except Ce) in hydrogenic micronodules are more easily transported into bioapatite fossils [62–64]. Compared with the Class I and III sediments, which do not have high REY contents, the REY-rich sediments (Class II) have higher contents of P_2O_5 , MnO, Fe_2O_3 , rock fragments, authigenic minerals, fish teeth, and sand. In addition, ΣREY of

both Class I and II sediments showed a strong positive correlation with P_2O_5 and MnO contents, a weak positive correlation with Fe_2O_3 , and a negative correlation with CaO/P_2O_5 (Figure 5), indicating that the carriers of REY in the samples are mainly coarse-grained minerals containing P, Mn, and Fe, such as fish teeth and micronodules. Combined with the geochemical data of other sediment samples from the Marcus-Wake Seamounts, it is clear that ΣREY has a good correlation with P_2O_5 , CaO/P_2O_5 , LREE/HREE, and δCe . However, as the REY content increases, the correlation between ΣREY and MnO and Fe_2O_3 becomes weaker, reflecting that the REY content of REY-rich sediments is mainly related to the content of bioapatite fossils, while the micronodules acted as intermediate carriers of REY in the early stage of sedimentation [59–63].

In summary, the REY in the surface sediments of the Marcus-Wake Seamounts partly derived from Asian dust and partly from seawater and/or porewater. The REY content of the sediments is mainly related to the quantity of fish teeth [6,8,62–64] and micronodules [11,59,60], which are intermediate carriers of REY in the early stage of sedimentation, and the REY will migrate from the micronodules to the fish teeth during diagenesis.

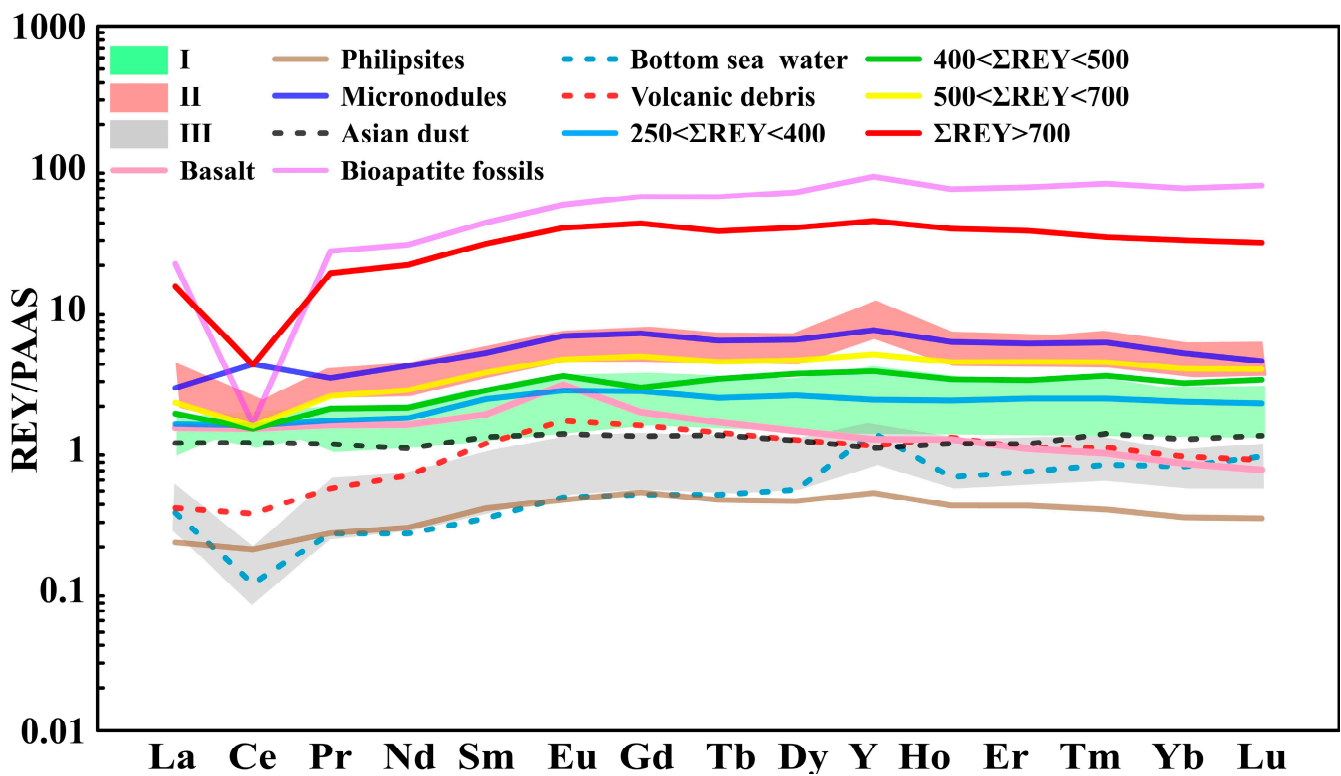


Figure 3. PAAS-normalized [44] REY pattern of all the samples in this study and some references. Asian dust (black dotted line) after [53–58]; Marcus-Wake Seamounts sediment (light blue, green, yellow and red lines) after [6,16,17]; micronodules (blue line), bioapatite fossils (purple line) and philipsites (brown line) after [6]; basalt (pink line) after [65]; bottom water (light blue dotted line) after [36], and volcanic debris (red dotted line) after [66].

4.3. Effect of Seamounts on REY Enrichment

Recently, the REY content in sediments and pore water near seamounts in the western and central Pacific Ocean has been found to be higher than that in abyssal plains far from seamounts, and REY content generally decreases with increasing distance from seamounts [9,10,19–21]. The 23° N latitude section in the study area is also characterized by a REY distribution that may be influenced by seamounts, as evidenced by the fact that ΣREY is higher in samples closer to seamounts (e.g., P13) than in samples far from seamounts (Figure 6c–f). In addition, the highest REY content occurs at station P11, which is located on the southeastern side of a large seamount, Niulang Guyot (see Figure 6a,b).

Bi et al. also found that the REY content of sediments from core C on the southeastern side of the Niulang Guyot is significantly higher than that from core B on the other side (Figure 6b), and that there is a REY-rich layer with a REY content of more than 2000 ppm in the lower part of core C [6].

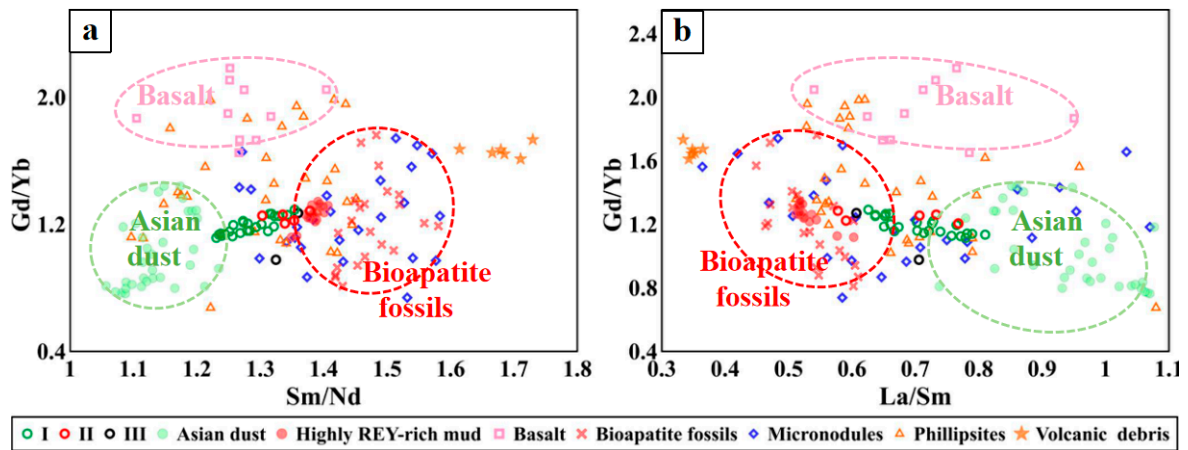


Figure 4. PAAS-normalized plot of Gd/Yb vs. Sm/Nd (a) and Gd/Yb vs. La/Sm (b) in the deep-sea sediments of this study (green, red and black circles) and other possible REY sources. Asian dust (green solid circle) after [53–58]; highly REY-rich mud (red solid circle) after [6,16,17]; basalt (pink square) after [65]; micronodules (blue diamond), bioapatite fossils (red cross) and philipsites (orange triangle) after [6], and volcanic debris (orange pentagram) after [66].

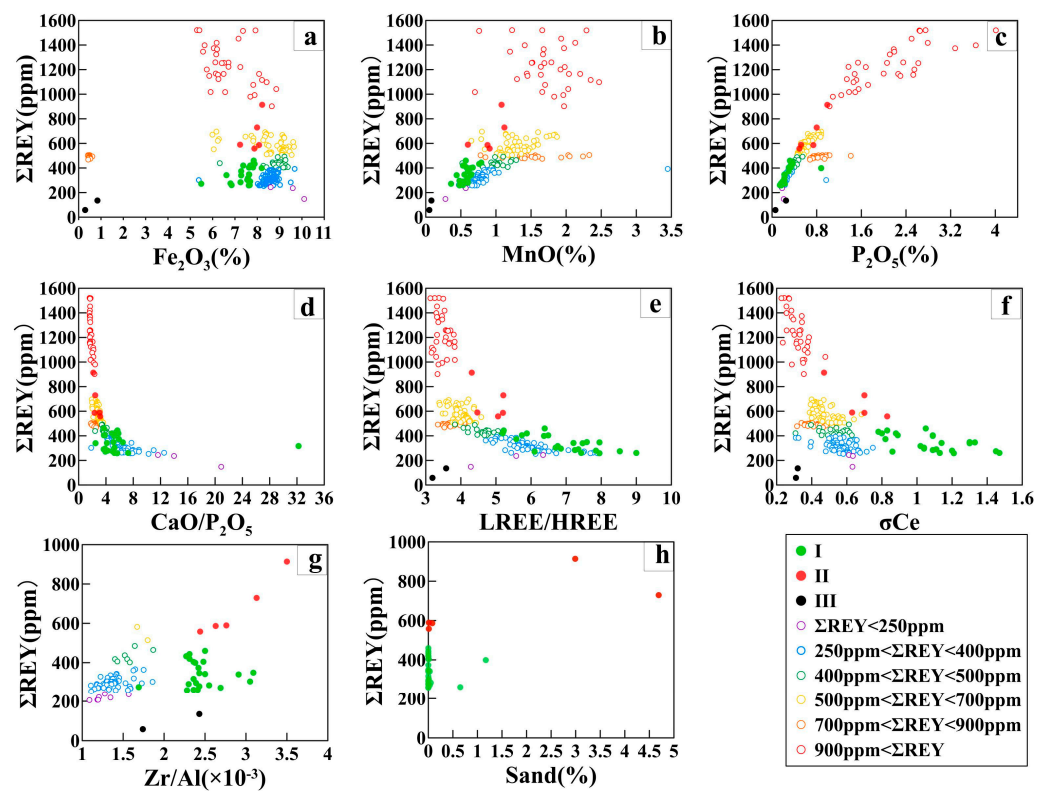


Figure 5. Relationship between REY and Fe₂O₃ (a), MnO (b), P₂O₅ (c), CaO/P₂O₅ (d), LREE/HREE (e), σCe (f), Zr/Al (g), sand (biosilicone free, (h)). I, II, III are samples of this study. Colored circles in (a–g) are 0–2 m averaged data and 0–25 cm data of sediments in the Marcus-Wake Seamounts, especially near Minamitorishima Island [6,16,17], respectively.

There are several reasons why the presence of seamounts may affect the distribution of REY in sediments. First, the interaction between seawater and seamounts often creates specialized current fields, such as Taylor columns, jet flows, upwelling, and eddies around seamounts, which promote seawater mixing and improve nutrient conditions in the vicinity of seamounts, making seamounts area more productive than abyssal plains [9,10,23,24,67,68] and facilitating the formation of bioapatite fossils. Second, the weathering process of seamount materials can supply REY to the surrounding seawater and pore water, increasing the flux of REY and facilitating the formation of REY-rich sediments [19,23]. Finally, the geological and hydrodynamic environments around seamounts are more favorable for the formation of REY-rich sediments. Ohta et al. suggested that stronger bottom currents may lead to the selective accumulation of REY-enriched coarse grains, such as bioapatite fossils, resulting in the formation of REY-rich sediments [3]. Shi et al. also suggested that the REY-rich sediments are mostly formed in deep-sea areas subject to low deposition rates and erosion by oxygen-enriched bottom currents [5]. Therefore, an environment with strong bottom currents and low sedimentation rates in the seamount area is favorable for the formation of REY-rich sediments.

The factors analyzed above, such as ocean productivity, seamount weathering, and hydrodynamics, are all strongly related to the current field around seamounts. The results of numerical simulations in the seamount area of the northwest Pacific Ocean show that mesoscale eddies often occur near Caiwei Guyot, Weijia Guyot, and Niulang Guyot, and the clockwise bottom currents around the seamounts are more developed and tend to be stronger toward the southeast of the seamounts [23]. Nearly one year of observations are available from a mooring system located southeast of Niulang Guyot (water depth 5050 m), not far from core C [69]. The main direction and average velocity of the bottom current observed by the current meter deployed in the 4920 m layer were southwest and 10.1 cm/s, respectively [69]. This current velocity can cause sediment resuspension [70], which is conducive to the elution of clays that dilute the REY content and accelerate the redistribution of REY in various media. In addition, prolonged seafloor erosion can cause landslides around seamounts [71], and similar processes will transport coarse-grained materials (including rock fragments, authigenic minerals, bioapatite fossils, etc.) into the surrounding area. We found abundant rock fragments in samples P11 and P12 from the southeastern flank of Niulang Guyot, which also indicates that the nearby depositional environment is unstable and there is a possibility of landslide events. Turnewitsch et al. investigated the relationship between the composition of the sediments in the seamount region and the strength of the current and found that the Zr/Al of the sediments increased with the strength of the current [72]. The Σ REY of our samples have a positive correlation with Zr/Al (Figure 5g), indicating that stronger bottom currents are likely to be present where the REY content is high, which is consistent with the previous assessment [3,6,10,16,17]. Strong bottom currents may coarsen the sediment grains. Higher Σ REY corresponds to higher sand content (biosilicon free) (Figure 5h), suggesting that higher Σ REY may also indicate stronger bottom currents to some extent. In addition, strong bottom currents are unfavorable for TOC preservation, and the low TOC contents in P11 and P12 confirm that there may be stronger bottom currents at P11 and P12 where REY contents are high and even the modern deposits may be missing due to erosion.

The results of this study indicate that REY-rich sediments are more likely to occur in the southeastern direction of large seamounts (e.g., Niulang Guyot). The REY-rich sediments in the area near Minamitorishima Island are also mainly located in the southeastern direction of a large seamount-Takuyo Daigo Seamount (Figure 6b). In summary, the southeastern direction of some large seamounts in the western Pacific Ocean may have strong bottom currents that can selectively enrich the REY-rich bioapatite fossils and micronodules to form REY-rich sediments.

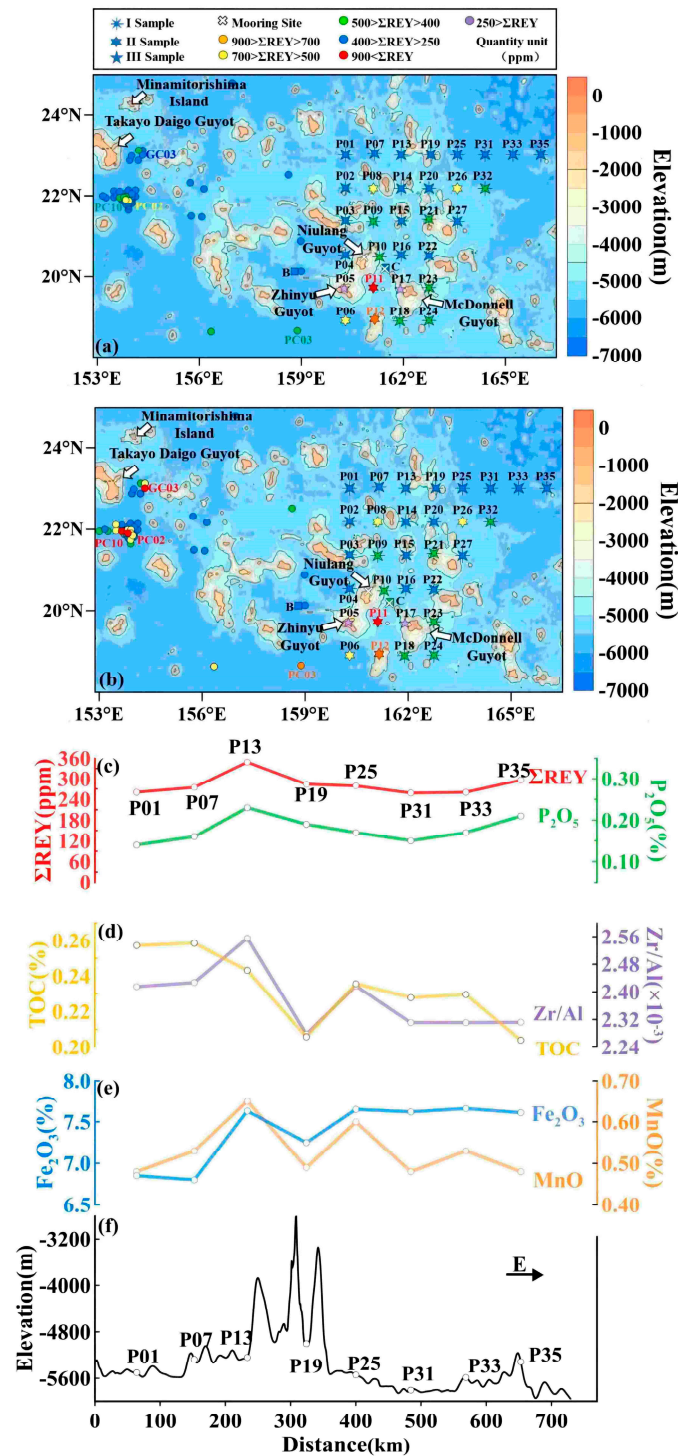


Figure 6. Distribution of Σ REY (ppm) in surficial (0–25 cm) sediment (a) and 0–2 m sediment (b), and the changes of Σ REY, P₂O₅ (c), TOC, Zr/Al (d) Fe₂O₃, MnO (e) along profile 23° N (f). I, II, III, this study; data of filled circles after [6,16,17]; bold cross shows the mooring site [69]. Note that: (1) higher Σ REY were found at stations southeast of large seamounts such as Niulang Guyot and Takayo Daigo Seamount; (2) along the 23° N profile, stations near seamounts (e.g., P13) have higher levels of Σ REY, P₂O₅, Fe₂O₃, MnO, and Zr/Al, while stations farther from seamounts (e.g., P31, P33) have lower levels of these values.

5. Conclusions

First, the geochemical composition of the surface sediments in the study area is mainly controlled by the input of terrestrial and seamount-derived detritus, calcareous and siliceous biogenic detritus, and to a lesser extent by the formation of authigenic minerals (e.g., micronodules) and bioapatite fossils. The samples of this study can be categorized into Class I sediments ($n = 24$) with moderate REY content ($250 \text{ ppm} < \Sigma\text{REY} < 460 \text{ ppm}$) dominated by terrestrial detrital contributions, Class II sediments ($n = 5$) rich in REY ($\Sigma\text{REY} > 550 \text{ ppm}$) and authigenic minerals, and Class III sediments ($n = 2$) rich in CaCO_3 but poor in REY ($\Sigma\text{REY} < 250 \text{ ppm}$).

Second, the REY in the surface sediments of the Marcus-Wake Seamounts partly derived from Asian dust and partly from seawater and/or porewater and are enriched in carrier particles such as bioapatite fossils and micronodules. The REY content of these sediments is mainly related to the amount of bioapatite fossils and micronodules.

Finally, the presence of seamounts is conducive to the formation of REY-rich sediments. Strong bottom currents may exist in the southeastern direction of some large seamounts (e.g., Niulang Guyot), which can lead to the selective accumulation of REY-rich bioapatite fossils and micronodules, thus forming REY-rich sediments. In order to better understand the role of seamounts in the formation of REY-rich sediments, it is necessary to intensify in situ observations of the current field in the seamount area in the future.

Supplementary Materials: The following supporting information can be downloaded at: <https://www.mdpi.com/article/10.3390/jmse12010117/s1>, Table S1: Results of surface sediment grain size analyses, Table S2: Results of surface sediment geochemistry analyses, Table S3: Results of correlation; Table S4: Cluster analysis results.

Author Contributions: Conceptualization, T.X. and D.X.; methodology, D.X., L.Y. and Y.D.; software, T.X.; formal analysis, T.X. and D.X.; validation, D.X., L.Y., Q.G., X.H. and F.C.; writing original draft preparation, T.X., D.X., T.D. and J.L.; writing review and editing, T.X. and D.X.; visualization, T.X. and D.X.; funding acquisition, D.X. All authors have read and agreed to the published version of the manuscript.

Funding: This research was funded by the National Programme on Global Change and Air Sea Interaction (GASI-04-HYDZ-02 and GASI-01-CNPAC-CJ01), and the National Natural Science Foundation of China (No. 41427803).

Institutional Review Board Statement: Not applicable.

Informed Consent Statement: Not applicable.

Data Availability Statement: Data are available on request from the corresponding author D.X. (xudong@sio.org.cn).

Acknowledgments: We thank the crew onboard RV Xiangyanghong 10 for collecting samples during the DY54 cruise. We are grateful to John S. Armstrong-Altrin, and other two anonymous reviewers for their detailed and constructive comments.

Conflicts of Interest: The authors declare no conflict of interest.

References

1. Kato, Y.; Fujinaga, K.; Nakamura, K.; Takaya, Y.; Kitamura, K.; Ohta, J.; Toda, R.; Nakashima, T.; Iwamori, H. Deep-sea mud in the Pacific Ocean as a potential resource for rare-earth elements. *Nat. Geosci.* **2011**, *4*, 535–539. [[CrossRef](#)]
2. Iijima, K.; Yasukawa, K.; Fujinaga, K.; Nakamura, K.; Machida, S.; Takaya, Y.; Ohta, J.; Haraguchi, S.; Nishio, Y.; Usui, Y.; et al. Discovery of extremely REY-rich mud in the western North Pacific Ocean. *Geochem. J.* **2016**, *50*, 557–573. [[CrossRef](#)]
3. Ohta, J.; Yasukawa, K.; Machida, S.; Fujinaga, K.; Nakamura, K.; Takaya, Y.; Iijima, K.; Suzuki, K.; Kato, Y. Geological factors responsible for REY-rich mud in the western North Pacific Ocean: Implications from mineralogy and grain size distributions. *Geochem. J.* **2016**, *50*, 591–603. [[CrossRef](#)]
4. Yasukawa, K.; Ohta, J.; Mimura, K.; Tanaka, E.; Takaya, Y.; Usui, Y.; Fujinaga, K.; Machida, S.; Nozaki, T.; Iijima, K.; et al. A new and prospective resource for scandium: Evidence from the geochemistry of deep-sea sediment in the western North Pacific Ocean. *Ore Geol. Rev.* **2018**, *102*, 260–267. [[CrossRef](#)]

5. Shi, X.; Bi, D.; Huang, M.; Yu, M.; Luo, Y.; Zhou, T.; Zhang, Z.; Liu, J. Distribution and metallogenesis of deep-sea rare earth elements. *Geol. Bull. China* **2021**, *40*, 195–208. (In Chinese)
6. Bi, D.; Shi, X.; Huang, M.; Yu, M.; Zhou, T.; Zhang, Y.; Zhu, A.; Shi, M.; Fang, X. Geochemical and mineralogical characteristics of deep-sea sediments from the western North Pacific Ocean: Constraints on the enrichment processes of rare earth elements. *Ore Geol. Rev.* **2021**, *138*, 104318. [[CrossRef](#)]
7. Nakamura, K.; Fujinaga, K.; Yasukawa, K.; Takaya, Y.; Ohta, J.; Machida, S.; Haraguchi, S.; Kato, Y. Chapter 268—REY-Rich Mud: A Deep-Sea Mineral Resource for Rare Earths and Yttrium. In *Handbook on the Physics and Chemistry of Rare Earths*; Bünzli, J.G., Pecharsky, V.K., Eds.; Elsevier Science Ltd.: Amsterdam, The Netherlands, 2015; Volume 46, pp. 79–127.
8. Kashiwabara, T.; Toda, R.; Nakamura, K.; Yasukawa, K.; Fujinaga, K.; Kubo, S.; Nozaki, T.; Suzuki, K.; Kato, Y. Synchrotron X-ray spectroscopic perspective on the formation mechanism of REY-rich muds in the Pacific Ocean. *Geochim. Cosmochim. Acta* **2018**, *240*, 274–292. [[CrossRef](#)]
9. Ohta, J.; Yasukawa, K.; Nakamura, K.; Nozaki, T.; Takaya, Y.; Mimura, K.; Fujinaga, K.; Nakamura, K.; Usui, Y.; Kimura, J.; et al. Fish proliferation and rare-earth deposition by topographically induced upwelling at the late Eocene cooling event. *Sci. Rep.* **2020**, *18*, 9896. [[CrossRef](#)]
10. Ohta, J.; Yasukawa, K.; Nakamura, K.; Fujinaga, K.; Iijima, K.; Kato, Y. Geological features and resource potential of deep-sea mud highly enriched in rare-earth elements in the Central Pacific Basin and the Penrhyn Basin. *Ore Geol. Rev.* **2021**, *139*, 104440. [[CrossRef](#)]
11. Zhou, T.; Shi, X.; Huang, M.; Yu, M.; Bi, D.; Ren, X.; Yang, G.; Zhu, A. The Influence of Hydrothermal Fluids on the REY-Rich Deep-Sea Sediments in the Yupanqui Basin, Eastern South Pacific Ocean: Constraints from Bulk Sediment Geochemistry and Mineralogical Characteristics. *Minerals* **2020**, *10*, 1141. [[CrossRef](#)]
12. Haley, B.A.; Klinkhammer, G.P.; McManus, J. Rare earth elements in pore waters of marine sediments. *Geochim. Cosmochim. Acta* **2004**, *68*, 1265–1279. [[CrossRef](#)]
13. Schacht, U.; Wallmann, K.; Kutterolf, S. The influence of volcanic ash alteration on the REE composition of marine pore waters. *J. Geochem. Explor.* **2010**, *106*, 176–187. [[CrossRef](#)]
14. Yasukawa, K.; Liu, H.J.; Fujinaga, K.; Machida, S.; Haraguchi, S.; Ishii, T.; Nakamura, K.; Kato, Y. Geochemistry and mineralogy of REY-rich mud in the eastern Indian Ocean. *J. Asian Earth Sci.* **2014**, *93*, 25–36. [[CrossRef](#)]
15. Yasukawa, K.; Ohta, J.; Miyazaki, T.; Vaglarov, B.S.; Chang, Q.; Ueki, K.; Toyama, C.; Kimura, J.; Tanaka, E.; Nakamura, K.; et al. Statistic and Isotopic Characterization of Deep-Sea Sediments in the Western North Pacific Ocean: Implications for Genesis of the Sediment Extremely Enriched in Rare Earth Elements. *Geochem. Geophys. Geosystems* **2019**, *7*, 3402–3430. [[CrossRef](#)]
16. Tanaka, E.; Nakamura, K.; Yasukawa, K.; Minura, K.; Fujinaga, K.; Iijima, K.; Nozaki, T.; Kato, Y. Chemostratigraphy of deep-sea sediments in the western North Pacific Ocean: Implications for genesis of mud highly enriched in rare-earth elements and yttrium. *Ore Geol. Rev.* **2020**, *119*, 103392. [[CrossRef](#)]
17. Tanaka, E.; Nakamura, K.; Yasukawa, K.; Minura, K.; Fujinaga, K.; Ohta, J.; Iijima, K.; Nozaki, T.; Machida, S.; Kato, Y. Chemostratigraphic Correlations of Deep-Sea Sediments in the Western North Pacific Ocean: A New Constraint on the Distribution of Mud Highly Enriched in Rare-Earth Elements. *Minerals* **2020**, *10*, 575. [[CrossRef](#)]
18. Liao, J.; Sun, X.; Li, D.; Sa, R.; Lu, Y.; Lin, Z.; Xu, L.; Zhan, R.; Pan, Y.; Xu, H. New insights into nanostructure and geochemistry of bioapatite in REE-rich sediments: LA-ICP-MS, TEM, and Z-contrast imaging studies. *Chem. Geol.* **2019**, *512*, 58–68. [[CrossRef](#)]
19. Deng, Y.; Guo, Q.; Liu, C.; He, G.; Cao, J.; Liao, J.; Liu, C.; Wang, H.; Zhou, J.; Liu, Y.; et al. Early diagenetic control on the enrichment and fractionation of rare earth elements in deep-sea sediments. *Sci. Adv.* **2022**, *8*, eabn5466. [[CrossRef](#)]
20. Wang, F.; He, G.; Deng, X.; Yang, Y.; Ren, J. Fish Teeth Sr Isotope Stratigraphy and Nd Isotope Variations: New Insights on REY Enrichments in Deep-Sea Sediments in the Pacific. *J. Mar. Sci. Eng.* **2021**, *9*, 1379. [[CrossRef](#)]
21. Deng, Y.; Guo, Q.; Zhu, J.; He, G.; Yang, Y.; Cao, J.; Ren, J.; Liu, Y.; Famiyeh, L.; Guo, B.; et al. Significant contribution of seamounts to the oceanic rare earth elements budget. *Gondwana Res.* **2022**, *112*, 71–81. [[CrossRef](#)]
22. Turnewitsch, R.; Falahat, S.; Nycander, J.; Dale, A.; Scott, R.B.; Furnival, D. Deep-sea fluid and sediment dynamics—Influence of hill- to seamount-scale seafloor topography. *Earth Sci. Rev.* **2013**, *127*, 203–241. [[CrossRef](#)]
23. Jiang, X.; Dong, C.; Ji, Y.; Wang, C.; Shu, Y.; Liu, L.; Ji, J. Influences of Deep-Water Seamounts on the Hydrodynamic Environment in the Northwestern Pacific Ocean. *J. Geophys. Res. Ocean.* **2021**, *126*, e2021JC017396. [[CrossRef](#)]
24. Ezer, T. On the Interaction between the Gulf Stream and the New England Seamount Chain. *J. Phys. Oceanogr.* **1994**, *24*, 191–204. [[CrossRef](#)]
25. Roden, G.I. Effect of seamounts and seamount chains on ocean circulation and thermohaline structure. *Seamounts Isl. Atolls* **1987**, *43*, 335–354.
26. Holmes, R.M.; Laverne, C.D.; McDougall, T. Ridges, seamounts, troughs, and bowls: Topographic control of the dianeutral circulation in the Abyssal Ocean. *J. Phys. Oceanogr.* **2018**, *48*, 861–882. [[CrossRef](#)]
27. Bi, D.; Shi, X.; Huang, M.; Yu, M.; Shen, F.; Liu, J.; Zhou, T.; Chen, T.; Shi, F.; Wang, X.; et al. Dating Pelagic Sediments from the Northwestern Pacific Ocean by Integration of Multi-geochronologic Approaches. *Ore Geol. Rev.* **2023**, *161*, 105614. [[CrossRef](#)]
28. Koppers, A.A.; Staudigel, H.; Pringle, M.S.; Wijbrans, J.R. Short-lived and discontinuous intraplate volcanism in the South Pacific: Hot spots or extensional volcanism? *Geochem. Geophys. Geosystems* **2003**, *4*, 1089. [[CrossRef](#)]
29. Xu, J.; Zheng, Y.; Bao, G.; Wu, X.; Zhang, K.; Jin, X. Research of seamount micro-topography based on acoustic deep-tow system investigation: A case from the Marcus-Wake Ridge area. *J. Mar. Sci.* **2011**, *29*, 17–24. (In Chinese)

30. Weiss, T.L.; Linsley, B.K.; Gordon, A.L. Pacific North Equatorial Current bifurcation latitude and Kuroshio Current shifts since the Last Glacial Maximum inferred from a Sulu Sea thermocline reconstruction. *Quat. Sci. Rev.* **2021**, *264*, 106999. [[CrossRef](#)]
31. Kawabe, M.; Fujio, S. Pacific ocean circulation based on observation. *J. Oceanogr.* **2010**, *66*, 389–403. [[CrossRef](#)]
32. Kawabe, M.; Fujio, S.; Yanagimoto, D. Deep-water circulation at low latitudes in the western North Pacific. *Deep Sea Res. Part I Oceanogr. Res. Pap.* **2003**, *50*, 636–656. [[CrossRef](#)]
33. Kawabe, M.; Fujio, S.; Yanagimoto, D.; Tanaka, K. Water masses and currents of deep circulation southwest of the Shatsky Rise in the western North Pacific. *Deep Sea Res. Part I Oceanogr. Res. Pap.* **2009**, *56*, 1675–1681. [[CrossRef](#)]
34. Hu, R.; Piotrowski, A.M. Neodymium isotope evidence for glacial-interglacial variability of deepwater transit time in the Pacific Ocean. *Nat. Commun.* **2018**, *9*, 4709. [[CrossRef](#)] [[PubMed](#)]
35. Frey, F.A.; Coffin, M.; Wallace, P.J.; Quilty, P.G. *Proceedings of the Ocean Drilling Program, Scientific Results. Vol. 183. Kerguelen Plateau-Broken Ridge: A Large Igneous Province: Covering Leg 183 DV "Joides Resolution"*; Texas A&M University Ocean Drilling Program: College Station, TX, USA, 2003; pp. 1135–1142.
36. Deng, Y.; Ren, J.; Guo, Q.; Cao, J.; Wang, H.; Liu, C. Geochemistry characteristics of REY-rich sediment from deep sea in Western Pacific, and their indicative significance. *Acta Petrol. Sin.* **2018**, *34*, 733–747. (In Chinese)
37. Deng, Y.; Ren, J.; Guo, Q.; Wang, H.; Yu, Z.; Liu, C. Trace Elements Geochemistry Characteristics of Seawater and Porewater in Deep-Water Basin, Western Pacific. *Earth Sci.* **2019**, *44*, 3102–3114. (In Chinese)
38. Qiu, Z.; Ma, W.; Zhang, X.; Ren, J. Geochemical characteristics of sediments in the southeast sea area of Minamitorishima Island and their indication of rare earth elements resources. *Geol. Sci. Technol. Inf.* **2019**, *38*, 205–214. (In Chinese)
39. Qiu, Z.; Ma, W.; Zhang, X.; Dong, Y.; Zhang, W.; Yang, K. Geochemical characteristics of surface sediments in the northwestern Pacific and their indication of materials sources. *J. Zhejiang Univ. (Sci. Ed.)* **2020**, *47*, 345–369. (In Chinese)
40. Luo, S.; Ren, J.; He, G.; Deng, X. Geochemical Characteristics of Polymetallic Nodules and Their Surface Sediments in the Western Pacific: Effect of Sedimentary Environment on Nodule Growth. *Mar. Geol. Quat. Geol.* **2023**, *43*, 119–135. (In Chinese)
41. Ren, J.; He, G.; Yao, H.; Zhang, H.; Yang, S.; Deng, X.; Zhu, K. Geochemistry and Significance of REE and PGE of the Cobalt-Rich Crusts from West Pacific Ocean Seamounts. *Earth Sci.* **2016**, *41*, 1745–1757. (In Chinese)
42. Yi, L.; Hu, B.; Zhao, J.; Jiang, X.; Shu, Y.; Wang, X.; Guo, J.; Wang, F.; Ding, X.; Liu, G.; et al. Magneto stratigraphy of Abyssal Deposits in the Central Philippine Sea and Regional Sedimentary Dynamics During the Quaternary. *Paleoceanogr. Paleoclimatol.* **2022**, *37*, e2021PA004365. [[CrossRef](#)]
43. Taylor, S.R.; McLennan, S.M. *The Continental Crust: Its Composition and Evolution: An Examination of the Geochemical Record Preserved in Sedimentary Rocks*; Blackwell: London, UK, 1985; pp. 57–72.
44. Pourmand, A.; Dauphas, N.; Ireland, T.J. A novel extraction chromatography and MC-ICP-MS technique for rapid analysis of REE, Sc and Y: Revising CI-chondrite and Post-Archean Australian Shale (PAAS) abundances. *Chem. Geol.* **2012**, *291*, 38–54. [[CrossRef](#)]
45. Dunlea, A.G.; Murray, R.W.; Sauvage, J.; Spivack, A.J.; Harris, R.N.; D'Hondt, S. Dust, volcanic ash, and the evolution of the South Pacific Gyre through the Cenozoic. *Paleoceanography* **2015**, *30*, 1078–1099. [[CrossRef](#)]
46. Yuan, C.; Meng, F.; Yao, Y.; Ni, J. Geochemical speciation and spatial distributions of phosphorus in surface sediments from the basin of the Marcus-Wake seamounts in the western Pacific Ocean. *Acta Oceanol. Sin.* **2022**, *41*, 80–90. [[CrossRef](#)]
47. Dymond, J.; Suess, E.; Lyle, M. Barium in Deep-Sea Sediment: A Geochemical Proxy for Paleoproductivity. *Paleoceanography* **1992**, *7*, 163–181. [[CrossRef](#)]
48. Zhang, J.; Meng, X.; Xia, P. The Ba cycle during the early diagenesis of deep-sea sediments and its implication for paleoceanographical environmental. *Adv. Mar. Sci.* **2009**, *27*, 275–280. (In Chinese)
49. McLennan, S.M. Rare earth elements in sedimentary rocks: Influences of provenance and sedimentary processes. *Rev. Miner. Geochem.* **1989**, *21*, 169–200.
50. Cullers, R.L. The controls on the major and trace element variation of shales, siltstones sandstones of Pennsylvanian-Permian age from uplifted continental block in Colorado to platform sediment in Kansas, USA. *Geochim. Cosmochim. Acta* **1994**, *58*, 4955–4972. [[CrossRef](#)]
51. Honda, M.; Shimizu, H. Geochemical, mineralogical and sedimentological studies on the Taklimakan desert sands. *Sedimentology* **1998**, *45*, 1125–1143. [[CrossRef](#)]
52. Cullers, R.L.; Barrett, T.; Carlson, R.; Robinson, B. Rare-earth element and mineralogical changes in Holocene soil and stream sediment: A case study in the Wet Mountains, Colorado, USA. *Chem. Geol.* **1987**, *63*, 275–297. [[CrossRef](#)]
53. Ming, B.; Sylvain, G.; Han, J. Geochemistry of the Xining, Xifeng and Jixian sections, Loess Plateau of China: Eolian dust provenance and paleosol evolution during the last 140 ka. *Chem. Sci.* **2000**, *178*, e2021PA004365.
54. Li, Y.; Liang, P.; Song, Y.; Li, X.; Yang, S.; Chen, X.; Zong, X.; Shukurov, N.; Li, Y. Unraveling source-to-sink dust transport in Central and East Asia by identifying provenances of aeolian sediments. *Atmos. Res.* **2023**, *293*, 106929. [[CrossRef](#)]
55. Chen, Q.; Li, Z.; Dong, S.; Wang, N.; Lai, D.; Ning, K. Spatial Variations in the Chemical Composition of Eolian Sediments in Hyperarid Regions: A Case Study from the Badain Jaran Desert, Northwestern China. *J. Sediment. Res.* **2018**, *88*, 290–300. [[CrossRef](#)]
56. Chen, X.; Song, Y.; Li, Y.; Huang, Y.; Zhou, X.; Fan, Y. Provenance of sub-aerial surface sediments in the Tarim Basin, Western China. *Catena* **2020**, *198*, 105014. [[CrossRef](#)]

57. Jiang, Q.; Yang, X. Sedimentological and Geochemical Composition of Aeolian Sediments in the Taklamakan Desert: Implications for Provenance and Sediment Supply Mechanisms. *J. Geophys. Res. Earth Surf.* **2019**, *124*, 1217–1237. [[CrossRef](#)]
58. Zhao, W.; Sun, Y.; Balsam, W.; Lu, H.; Liu, L.; Chen, J.; Ji, J. Hf-Nd isotopic variability in mineral dust from Chinese and Mongolian deserts: Implications for sources and dispersal. *Sci. Rep.* **2014**, *4*, 5837. [[CrossRef](#)] [[PubMed](#)]
59. Zhang, H.; Zhou, J.; Yuan, P.; Dong, Y.; Fan, W.; Chu, F.; Xiao, W.; Liu, D. Highly positive Ce anomalies of hydrogenetic ferromanganese micronodules from abyssal basins in the NW and NE Pacific: Implications for REY migration and enrichment in deep-sea sediments. *Ore Geol. Rev.* **2023**, *154*, 105324. [[CrossRef](#)]
60. Liao, J.; Sun, X.; Wu, Z.; Sa, R.; Yao, G.; Lu, Y.; Li, D.; Liu, Y.; Deng, Y.; Pan, Y. Fe-Mn (oxyhydr)oxides as an indicator of REY enrichment in deep-sea sediments from the central North Pacific. *Ore Geol. Rev.* **2019**, *112*, 103044. [[CrossRef](#)]
61. Yasukawa, K.; Kino, S.; Azami, K.; Tanaka, E.; Minura, K.; Ohta, J.; Fujinaga, K.; Nakamura, K.; Kato, Y. Geochemical features of Fe-Mn micronodules in deep sea sediments of the western North Pacific Ocean: Potential for co-product metal extraction from REY-rich mud. *Ore Geol. Rev.* **2020**, *127*, 103805. [[CrossRef](#)]
62. Liao, J.; Chen, J.; Sun, X.; Wu, Z.; Deng, Y.; Shi, X.; Wang, Y.; Chen, Y.; Koschinsky, A. Quantifying the controlling mineral phases of rare-earth elements in deep-sea pelagic sediments. *Chem. Geol.* **2022**, *595*, 120792. [[CrossRef](#)]
63. Manceau, A.; Paul, S.; Simionovici, A.L.; Magnin, V.; Balvay, M.; Findling, N.; Rovezzi, M.; Muller, S.; Garbe-Schönberg, D.; Koschinsky, A. Fossils Bioapatites with Extremely High Concentrations of Rare Earth Elements and Yttrium from Deep-Sea Pelagic Sediments. *ACS Earth Space Chem.* **2022**, *6*, 2093–2103. [[CrossRef](#)]
64. Takahashi, Y.; Hayasaka, Y.; Morita, K.; Kashiwabara, E.; Nakada, R.; Marcus, M.A.; Kato, K.; Tanaka, K.; Shimizu, H. Transfer of rare earth elements (REE) from manganese oxides to phosphates during early diagenesis in pelagic sediments inferred from REE patterns, X-ray absorption spectroscopy, and chemical leaching method. *Geochem. J.* **2015**, *49*, 653–674. [[CrossRef](#)]
65. Wei, X.; Shi, X.; Xu, Y.G.; Castillo, P.R.; Zhang, Y.; Zhang, L.; Zhang, H. Mid-Cretaceous Wake seamounts in NW Pacific originate from secondary mantle plumes with Arago hotspot composition. *Chem. Geol.* **2022**, *587*, 120632. [[CrossRef](#)]
66. Wang, H.; Yi, L.; Deng, X.; He, G. Geochemical and Mineral Properties of Quaternary Deep-Sea Sediments in the Central-Tropical Pacific and Its Response to the Mid-Pleistocene Transition. *J. Mar. Sci. Eng.* **2021**, *9*, 1254. [[CrossRef](#)]
67. Ma, J.; Song, J.; Li, X.; Yuan, H.; Li, N.; Duan, L.; Wang, Q. Environmental characteristics in three seamount areas of the Tropical Western Pacific Ocean: Focusing on nutrients. *Mar. Pollut. Bull.* **2019**, *143*, 163–174. [[CrossRef](#)] [[PubMed](#)]
68. Ma, J.; Song, J.; Li, X.; Yuan, H.; Li, N.; Duan, L.; Wang, Q. Control factors of DIC in the Y3 seamount waters of the Western Pacific Ocean. *J. Oceanol.* **2020**, *38*, 1215–1224. [[CrossRef](#)]
69. Sun, X.; Chen, J.; Chen, B.; Lin, C.; Liu, Y.; Huang, J.; Pan, Z.; Zhou, K.; He, Q.; Kuang, F.; et al. The particle fluxes in sediment traps from Niulang Guyot area in the Northwest Pacific. *Acta Oceanol. Sin.* **2022**, *41*, 34–44. [[CrossRef](#)]
70. Beaulieu, S.E. Accumulation and fate of phytodetritus on the sea floor. *Oceanogr. Mar. Biol.* **2002**, *40*, 171–232.
71. Howe, J.A.; Stoker, M.S.; Masson, D.G.; Pudsey, C.J.; Morris, P.; Larter, R.D.; Bulat, J. Seabed morphology and the bottom-current pathways around Rosemary Bank seamount, northern Rockall Trough, North Atlantic. *Mar. Petrol. Geol.* **2006**, *23*, 165–181. [[CrossRef](#)]
72. Turnewitsch, R.; Reyss, J.; Chapman, D.C.; Thomson, J.; Lampitt, R.S. Evidence for a sedimentary fingerprint of an asymmetric flow field surrounding a short seamount. *Earth Planet. Sci. Lett.* **2004**, *222*, 1023–1036. [[CrossRef](#)]

Disclaimer/Publisher’s Note: The statements, opinions and data contained in all publications are solely those of the individual author(s) and contributor(s) and not of MDPI and/or the editor(s). MDPI and/or the editor(s) disclaim responsibility for any injury to people or property resulting from any ideas, methods, instructions or products referred to in the content.